Chemical Science

ROYAL SOCIETY OF CHEMISTRY

EDGE ARTICLE

Cite this: *Chem. Sci.*, 2021, **12**, 2097

All publication charges for this article have been paid for by the Royal Society of Chemistry

The synthesis of a chemically reactive and polymeric luminescent gel†‡

Upama Baruah[a] and Uttam Manna *[ab]

In the past, chemically reactive polymeric interfaces have been considered to be of potential interest for developing functional materials for a wide range of practical applications. Furthermore, the rational incorporation of luminescence properties into such chemically reactive interfaces could provide a basis for extending the horizon of their prospective utility. In this report, a simple catalyst-free chemical approach is introduced to develop a chemically reactive and optically active polymeric gel. Branched-polyethyleneimine (BPEI)-derived, inherently luminescent carbon dots (BPEI-CDs) were covalently crosslinked with pentaacrylate (5Acl) through a 1,4-conjugate addition reaction under ambient conditions. The synthesized polymeric gel was milky white under visible light; however, it displayed fluorescence under UV light. Additionally, the residual acrylate groups in the synthesized fluorescent gel allowed its chemical functionality to be tailored through facile, robust 1,4-conjugate addition reactions with primary-amine-containing small molecules under ambient conditions. The chemical reactivity of the luminescent gel was further employed for a proof-of-concept demonstration of portable and parallel 'ON'/'OFF' toxic chemical sensing (namely, the sensing of nitrite ions as a model analyte). First, the chemically reactive luminescent gel derived from BPEI-CDs was covalently post-modified with aniline for the selective synthesis of a diazo compound in the presence of nitrite ions. During this process, the color of the gel under visible light changed from white to yellow and, thus, the colorimetric mode of the sensor was turned 'ON'. In parallel, the luminescence of the gel under UV light was quenched, which was denoted as the 'OFF' mode of the sensor. This parallel and unambiguous 'ON'/'OFF' sensing of a toxic chemical (nitrite ions, with a detection limit of 3 μM) was also achieved even in presence of other relevant interfering ions and at concentrations well below the permissible limit (65 μM) set by the World Health Organization (WHO). Furthermore, this chemically reactive luminescent gel could be of potential interest in a wide range of basic and applied contexts.

Received 18th September 2020
Accepted 29th November 2020

DOI: 10.1039/d0sc05166g

rsc.li/chemical-science

Introduction

Chemically reactive polymeric interfaces, which have conventionally been synthesized *via* layer-by-layer (LBL) deposition,[1,2,8–10,12] chemical vapor deposition (CVD)[3–5] and other processes,[6,7,11,13–19] have been employed to design various practically relevant functionalized soft materials. The residual chemical reactivity of such interfaces allows the robust covalent association of different desired chemical functionalities, mainly *via* catalyst-assisted click reactions,[3–7,11,17,18] click-type ring opening reactions[1,2,8–10,12,13,15] and 1,4-conjugate addition reactions,[9,14,16,19] among others. In the past, the residual chemical reactivity has been utilized to design patterned interfaces,[1,6,7,10,15] bio-interfaces,[2–5,8,17,18] systems for the sustained release of small molecules,[9] systems with optimized durable and smart bio-inspired extreme liquid wettabilities,[11–14,16,19] *etc.* Furthermore, this type of chemically reactive system could be rationally integrated with appropriate functional nanomaterials to develop smart interfaces for potential applications in practically relevant scenarios.

Additionally, zero-dimensional carbon nanomaterials, widely known as carbon dots (CDs), have emerged as important functional materials for various relevant applications including catalysis,[20] electrochemistry,[21] cellular imaging,[22] nanomedicine,[23] drug delivery,[24] and photovoltaics[25–27] due to their easy and cost-effective synthesis, low toxicity, good biocompatibility, tunable optical properties, and high quantum yields.[20–27] Fluorescent CDs decorated with various chemical functionalities depending on the choice of precursors have been

[a]*Bio-Inspired Polymeric Materials Lab, Department of Chemistry, Indian Institute of Technology-Guwahati, Kamrup, Assam 781039, India*

[b]*Centre for Nanotechnology, Indian Institute of Technology-Guwahati, Kamrup, Assam 781039, India. E-mail: umanna@iitg.ac.in*

† This work is dedicated to Prof. David M. Lynn.

‡ Electronic supplementary information (ESI) available: Fig. S1–S8, showing detailed characterization of the BPEI-CDs, the progressive formation of CRFG with time, the changes in fluorescence intensity of AMFG at different pH levels, fluorescence image analysis of AMFG in the presence of various concentrations of nitrite ions using the software ImageJ, digital photographs of nitrite sensing using CRFG (control study), and the fluorescence lifetime decay of AMFG in the presence of different concentrations of nitrite ions. See DOI: 10.1039/d0sc05166g

introduced for ratiometric pH sensing[28] and the detection of toxic chemicals including mercury ions,[29] hydrogen peroxide,[30] cholesterol,[31] biothiols,[32] and Pb^{2+};[33] a selective change in the optical signal of the respective CDs in the solution phase confirmed the existence of the mentioned toxic chemicals. However, a major drawback of using carbon dots in the solution phase arises from the aggregation-induced quenching of their photoluminescence.[34,35] Although a freshly prepared dispersion of CDs may display high potential for the detection of several relevant toxic metal ions or molecules, aggregation-induced quenching of the photoluminescence of the CDs could lead to ambiguous results in the sensing process for stored/aged sensors in the solution phase. The eventual real-world application of such potential chemical sensors would be highly challenging. Thus, further design of CD-derived portable sensors is essential for the unambiguous and easy detection of toxic chemicals.

In the recent past, various prospective strategies have been adopted to prevent aggregation-induced self-quenching in CDs for the development of various functional materials.[36–40] In a seminal report, Zhou and co-workers[36] introduced a CD-based hybrid nanogel to avoid unwanted aggregation-induced perturbations in the fluorescence signal. The CDs were physically deposited in a polymeric gel network, and the resulting material was further employed for both bioimaging and drug delivery applications. A condensation reaction was adopted to prepare a self-standing silica-based gel in which luminescent carbon dots were covalently crosslinked with an appropriate orthosilicate to prevent the aggregation-induced luminescence quenching of CDs in the solid state.[37] Interestingly, a significant enhancement in the fluorescence intensity of CDs was achieved in the solid state by incorporating them in a hydrophobic gel network.[38] In another approach, CDs were dispersed in a polymeric matrix to develop a smart ink for prospective anticounterfeiting applications.[39] In 2019, Jelinek and co-workers[40] strategically developed CD-derived multicolor fluorescent self-healing gels, in which carbon dots that were produced from different aldehyde precursors were reacted with branched polyethylenimine through a Schiff base reaction between the aldehydes and amines. This material was further employed for a proof-of-concept application as a white-light-emitting material. However, to date, the integration of CDs into a readily chemically reactive matrix is unprecedented; such a chemical approach would be appropriate for the controlled tailoring of the desired chemical functionalities around the immobilized CDs at the chemically reactive interface.

In the past, various luminescent gels have been developed through the incorporation of external fluorophores, including various small fluorescent dyes, fluorescent conjugated polymers, lanthanide transition metal ions, and quantum dots.[41–47] However, the earlier reported gels are mostly inappropriate for post-tailoring of the gel chemistry without affecting the embedded luminescence.[41–47] The design of a chemically reactive luminescent gel that would allow the incorporation of different functionalities without affecting its luminescence properties is unprecedented. In the present report, we have introduced a self-standing, chemically reactive luminescent gel through the strategic use of a non-fluorescent polymer (*i.e.*, branched poly(ethyleneimine); BPEI) and a multifunctional cross-linker (*i.e.*, dipentaerythritol penta-acrylate; 5Acl). The polymer-derived carbon dots (CDs) readily react with 5 Acl through a 1,4-conjugate addition reaction under ambient conditions. The synthesized gel was found to be luminescent and remained loaded with residual acrylate groups, which made the BPEI-CDs-derived gel highly chemically reactive towards primary-amine-containing small molecules under ambient conditions; namely, the residual acrylate groups from the crosslinker make the gel chemically reactive. The residual chemical reactivity of the luminescent gel was employed for a proof-of-concept design of a portable and parallel 'ON'/'OFF' sensor for toxic chemicals in the solid state that does not require a sophisticated instrumental set-up. First, the chemically reactive, luminescent gel was reacted with aniline through a 1,4-conjugate addition reaction for the selective synthesis of a diazo compound in the presence of a model toxic chemical, namely, nitrite ions. The change in color and quenching of luminescence in the milky white luminescent gel under visible light and UV light, respectively, provides a facile basis for recognizing the presence of toxic chemicals with the naked eye. Further, analysis of the digital images of the gel allowed quantification of the amount of the toxic chemical (*i.e.*, below 10 μM), even in the presence of various relevant interfering ions.

Results and discussion

Synthesis of chemically reactive and fluorescent gel (CRFG)

In the past, 1,4-conjugate addition reaction between amine and acrylate functional groups has been a facile and robust chemical platform for (a) synthesizing small molecules and biodegradable polymers, (b) amplifying surface functional groups and (c) fabricating bio-interfaces.[48–51] Recently, the amine of branched polyethyleneimine (BPEI) was covalently reacted with the acrylate of dipentaerythritol penta-acrylate (5Acl) through a 1,4-conjugate addition reaction under ambient conditions to synthesize chemically reactive interfaces, which were tailored to have various extreme liquid (oil/water) wettabilities.[13,16,19] In the current design, this same Michael addition reaction has been strategically introduced to synthesize a chemically reactive and fluorescent gel (CRFG). A widely accepted standard hydrothermal approach was followed to prepare fluorescent carbon dots from BPEI, which are denoted as BPEI-CDs, as shown in Schemes 1A and B. Transmission electron microscope (TEM) imaging and the selected area electron diffraction (SAED) pattern confirmed the successful synthesis of polycrystalline nano-dots of BPEI. As shown in Fig. S1A and B,‡ the average particle size of the prepared BPEI-CDs was found to be 7.6 ± 0.8 nm from dynamic light scattering (DLS) analysis (Fig. S1C‡). Furthermore, the emission spectrum of the BPEI-CDs revealed the existence of fluorescence under UV light (Fig. S1D‡). Next, an optically transparent reaction mixture of fluorescent BPEI-CDs and 5 Acl slowly (over 90 minutes, see ESI for more details‡) transformed into a gel through the 1,4-conjugate addition reaction between the amine groups of the BPEI-CDs and acrylate groups of 5Acl under ambient conditions, as

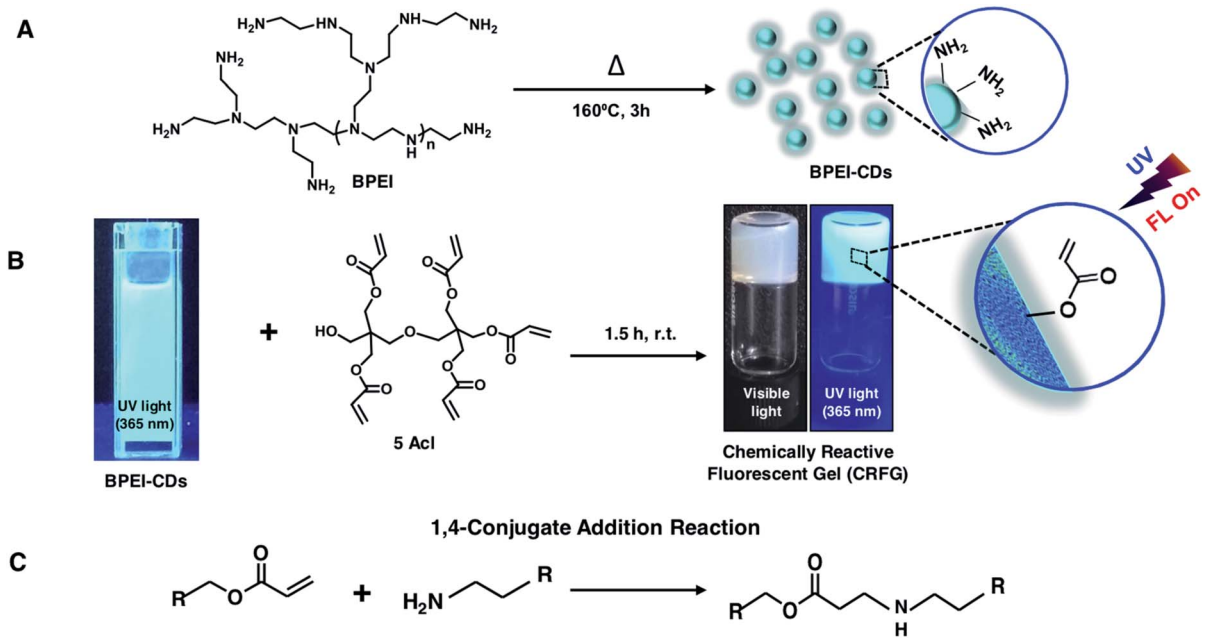

Scheme 1 (A) A schematic diagram depicting the synthesis of carbon dots from BPEI *via* a hydrothermal process. (B) The formation of a chemically reactive and fluorescent gel (CRFG) through a facile 1,4-conjugate addition reaction (C) between the amines of BPEI-CDs and acrylates of 5AcI under ambient conditions.

shown in Scheme 1B and Fig. S2A–G.‡ The synthesized CRFG was loaded with residual acrylate groups (Scheme 1B), which allowed the chemical functionality of the synthesized gel to be modulated *via* the desired primary-amine-containing small molecules *via* the same 1,4-conjugate addition reaction (Scheme 1B) under ambient conditions.

The morphology of the synthesized gel was investigated *via* a field emission scanning electron microscope (FESEM) study, whereas the existence of residual chemical reactivity and unaltered fluorescence were thoroughly characterized by visual inspection, fluorescence spectral and attenuated total reflectance Fourier transform infrared (ATR-FTIR) spectral analysis, as shown in Fig. 1A–L. The FESEM images of CRFG (Fig. 1C and E) revealed the presence of a uniformly connected porous network of globular nano-dots, as shown in Fig. 1E. Moreover, the synthesized gel, which was whitish under visible light, remained highly fluorescent under UV irradiation, as confirmed from the digital photographs (Fig. 1G and H respectively) and solid-state emission spectra (Fig. 1K; black line). The reaction mixture of BPEI-CDs and 5AcI was transformed into CRFG through the 1,4-conjugate addition reaction between amine and acrylate, as is evident from the ATR-FTIR analysis in Fig. S2H.‡ Upon the 1,4-conjugate addition reaction between the amine of BPEI-CDs and acrylate of 5AcI, only the vinyl moiety of the acrylate is compromised, as is evident from the ATR-FTIR spectral analysis of CRFG and 5AcI. A significant depletion in the IR peak intensity at 1410 cm^{-1} was observed with respect to the characteristic carbonyl stretch at 1726 cm^{-1}. As expected, the carbonyl moiety remained unaffected at the end of the 1,4-conjugate addition reaction, and the ATR-FTIR signature for the carbonyl stretch at 1726 cm^{-1} acts as an internal reference to monitor the covalent crosslinking between the BPEI-CDs and 5AcI. Furthermore, the existence of residual chemical reactivity in the synthesized gel was investigated using standard and widely accepted ATR-FTIR spectral analysis, as shown in Fig. 1L. The appearance of the characteristic IR peaks at 1410 cm^{-1} and 1726 cm^{-1} corresponding to the symmetric deformation of the C–H bond of the β-carbon of the vinyl group and ester carbonyl stretching, respectively, validated the presence of residual acrylate groups in CRFG. This residual chemical reactivity was utilized to modify the CRFG with aniline through a 1,4-conjugate addition reaction under ambient conditions. During this post-covalent modification process, the physical integrity and microscopic features of the gel remained unperturbed, as confirmed from FESEM imaging (Fig. 1C–F) and visual inspection (Fig. 1G–J).

Moreover, the fluorescence signal remained unaltered in the aniline-modified fluorescent gel (AMFG) compared to that of the native CRFG, as shown in Fig. 1H, J and K. The successful post-covalent modification of CRFG with aniline was investigated by comparing the ATR-FTIR spectra of CRFG and AMFG (Fig. 1L). The characteristic peak for the residual acrylate groups at 1410 cm^{-1} in AMFG was significantly depleted (blue spectrum, Fig. 1L) in comparison to that for CRFG (black spectrum, Fig. 1L); it should be noted that both IR spectra were normalized with respect to the ester carbonyl stretch appearing at 1726 cm^{-1}. During the 1,4-conjugate addition reaction between the amine and acrylate, only the vinyl moiety of the acrylate was compromised, whereas the carbonyl moiety remained unaffected at the end, and thus, the IR peak for carbonyl stretching acts as internal standard for monitoring the progress of the post-covalent reaction of the residual acylate groups of porous

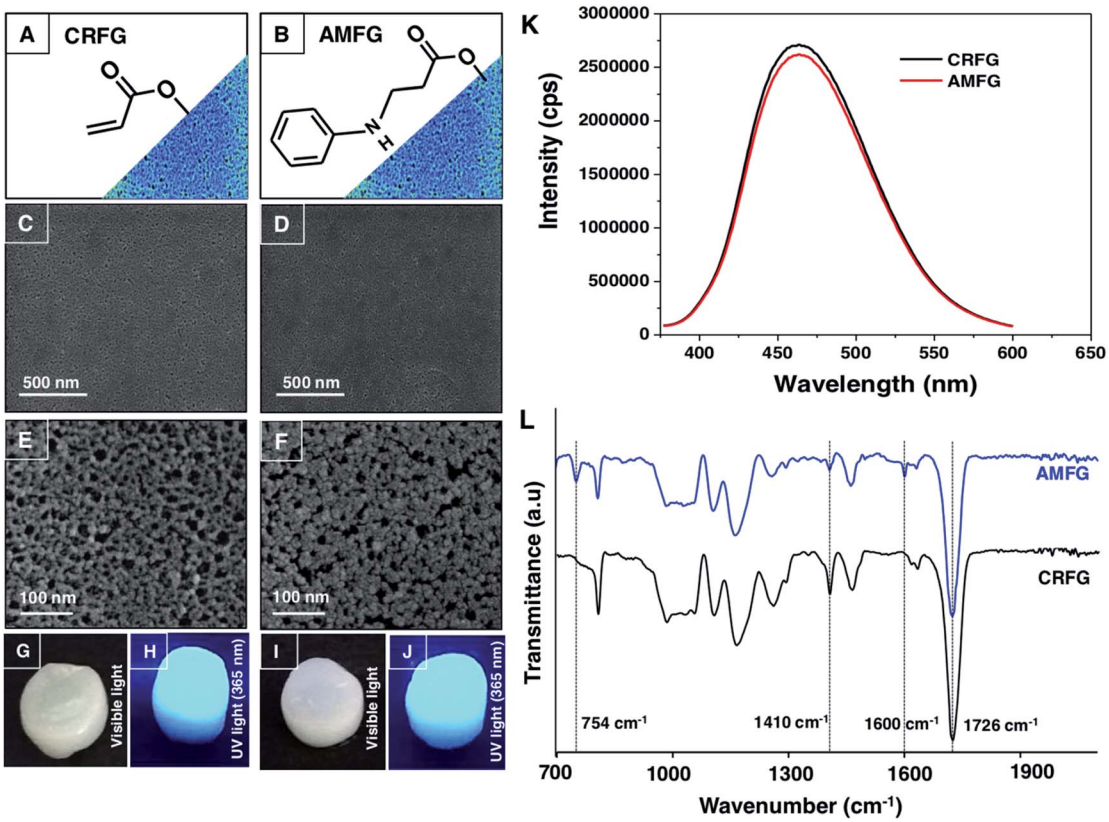

Fig. 1 Physical and chemical characterization of the chemically reactive fluorescent gel (CRFG) and aniline-modified fluorescent gel (AMFG). (A and B) Schematic diagrams representing the residual acrylate groups in CRFG (A) and the post-covalent modification of CRFG with aniline ((B) AMFG). FESEM images of CRFG (C and E) and AMFG (D and F) at lower (C and D) and higher (E and F) magnifications. The corresponding digital photographs of CRFG (G and H) and AMFG (I and J) under visible (G and I) and UV light ((H and J) 365 nm). (K and L) Comparisons of the fluorescence emission spectra (K) and attenuated total reflectance Fourier transform infrared (ATR-FTIR) spectra (L) of CRFG (black line) and AMFG (red line for fluorescence and blue line for the ATR-FTIR spectrum).

CRFG with a primary-amine-containing small molecule (*i.e.*, aniline). Furthermore, after the post-covalent modification of CRFG with aniline, two additional IR peaks were observed at 754 cm^{-1} and 1600 cm^{-1}, which are characteristic IR signatures for C–H (aromatic) out-of-plane ('oop') bending and aromatic C–C (in ring) stretching of the aromatic ring of aniline.[52] This simple comparative IR study unambiguously revealed the successful post-chemical modification of CRFG with the amine groups of aniline. This chemical avenue was further extended to develop a proof-of-concept design for a portable and parallel 'ON'/'OFF' sensor, in which unambiguous and facile detection of a toxic chemical was achieved without using a sophisticated instrumental set-up.

Design of a parallel and portable 'ON'/'OFF' sensor

The inappropriate use of nitrogenous fertilizers for plant growth, antiseptics for inhibiting microbial contamination in preserved meat and colour retention agents in the food processing industry continuously contribute to elevating the NO_2^- levels in drinking water beyond the permissible limit.[53,54] The consumption of high concentrations of nitrites is known to cause esophageal and stomach cancer, shortness of breath, tissue hypoxia and serious medical disorders (*e.g.*, blue baby syndrome or methemoglobinaemia).[53–58] The World Health Organization (WHO) has set the maximum limit for NO_2^- in drinking water as 65 μM.[53,59,60] Thus, it is of utmost importance to develop a portable sensor for the facile and unambiguous detection of the nitrite level in drinking water even in remote places, where the availibility of sophisticated instrumentation is limited. To date, various solution-phase analytical methods, including electrochemical techniques,[61–63] spectrophotometry,[64,65] chemiluminescence,[66,67] fluorescence spectrometry,[68–71] capillary electrophoresis,[72,73] ion chromatography,[74] and surface-enhanced Raman scattering[75] have been introduced for the detection of NO_2^- in aqueous environments. In comparison, fluorescence spectrometric and colorimetric methods have emerged as more convenient techniques for nitrite detection. In the recent past, various nanomaterials, including carbon dots,[76–79] dye-doped silica nanoparticles,[60] polyethyleneimine-capped CdS quantum dots,[75] 4-aminothiophenol-modified gold nanorods,[80] a graphite-like carbon nitride nanomaterial,[81] an *o*-phenylenediamine-BODIPY probe,[82] inorganic complexes such as iron and manganese pyridoxal-based complexes,[83] polymeric matrices,[84,85] metal–organic frameworks,[86] and functionalized gold and silver nanoparticles[87–91] have been developed for the

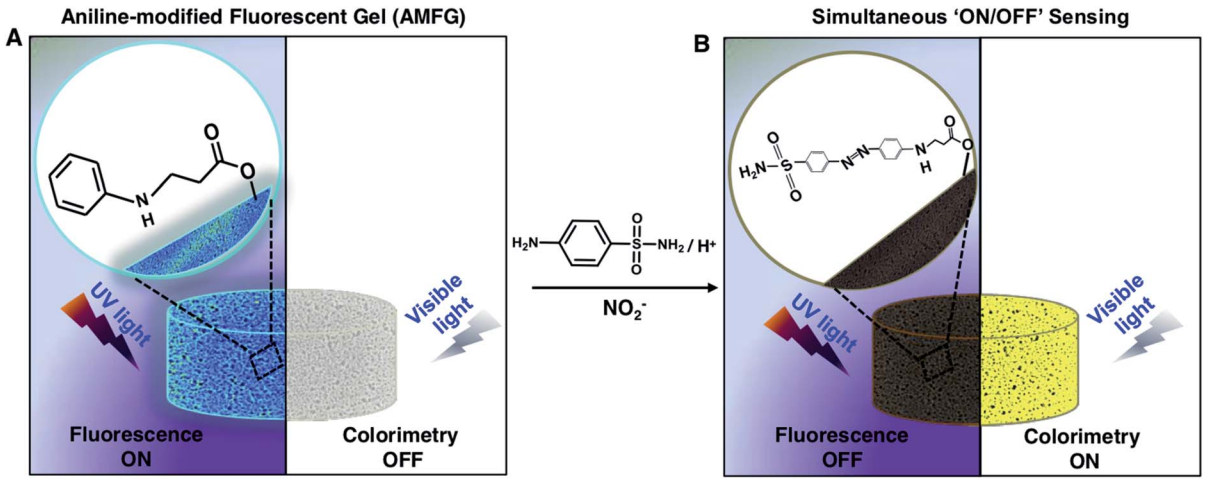

Scheme 2 A schematic representation of AMFG under visible and UV light (365 nm) before (A) and after (B) the parallel 'ON'/'OFF' sensing of NO_2^- in the presence of sulfanilamide. The formation of the diazo dye in the porous gel led to a simultaneous change in color (white to yellow; colorimetric mode is 'ON') and the fluorescence signal (quenched from blue to dark; fluorometric mode is 'OFF') under visible light and UV light, respectively.

colorimetric and fluorescence-based detection of NO_2^-. However, over time, the aggregation of nanomaterials in the solution phase is likely to lead to ambiguity in the measurement of the respective optical signals in various practically relevant settings. Therefore, despite significant progress, the design of a portable and stable sensor for nitrite detection has remained a practical challenge. Further, the development of a nitrite sensor for unambiguous and regular on-site monitoring of drinking water in remote places is essential.

To combat this practically relevant challenge, in the current study, AMFG is employed for portable, facile dual-mode (parallel 'ON' and 'OFF' of two distinct signals) sensing of nitrite ions. In the past, the modified Griess reaction has been used extensively in the development of assays to detect nitrite ions, in which sulfanilamide and *N*-(1-naphthyl) ethylenediamine were used as primary reagents. The sulfanilamide molecules are converted to diazonium cations in the presence of nitrite ions under acidic conditions, and subsequently couple with *N*-(1-naphthyl) ethylenediamine. The resulting colored diazo compound indicates the presence of nitrite ions in the solution phase. Inspired by this modified Griess reaction, AMFG with covalently immobilized aniline (a whitish, porous gel, as shown in Scheme 2A) was employed to synthesize a colored diazo compound in the porous gel as shown in Scheme 2B. The mixture of NO_2^- and sulfanilamide molecules readily reacted in acidic media to yield a colorless diazonium cation. Subsequently, the covalently immobilized aniline moiety of AMFG mutually and rapidly reacted with this colorless diazonium cation to form a yellow-colored diazo dye that remained covalently attached to the gel network, as shown in Scheme 2B. During this reaction process, the color of the gel under visible light changed from white to yellow, and simultaneously, the fluorescence signal of the gel was quenched under UV light, as shown in Schemes 2A and B. Thus, the simultaneous changes in the (a) colorimetric and (b) fluorometric modes in the AMFG were denoted as 'ON'/'OFF' sensing of nitrite in the solid state. The polymer-derived carbon dots used in our design are covalently integrated with the acrylate groups of 5-Acl through a single-step 1,4-conjugate addition reaction under ambient conditions without the use of any catalyst or initiator. This covalent integration allowed a durable gel to be achieved. It should be mentioned here that the fluorescence intensity of AMFG remained unaffected over the entire pH range from pH 1–14, as shown in Fig. S3 (ESI‡), which enabled the sensing of NO_2^- using AMFG in low pH media without any ambiguity. Moreover, it was observed that the fluorescence intensity of the synthesized gel varied only slightly (11.2% decrease compared to day 0), even after submerging the prepared gel in water for 90 days, as demonstrated in Fig. S4.‡ Furthermore, the AMFG gels exhibited two distinct changes: (1) the appearance of color of the gel under visible light and (2) quenching of the fluorescence under UV light depending on the concentration (3–21 μM) of NO_2^- present during the analysis process, as shown in Fig. 2A and B.

The appearance of an intense yellow color and the complete disappearance of the fluorescence signal in the gel were observed at a concentration of 21 μM, which is far below the toxic level of NO_2^- set by WHO.[59] Further, the synthesis of the yellow diazo compound in AMFG was characterized using ATR spectral analysis before and after the Griess reaction. The ATR spectrum of AMFG after the reaction with the reaction mixture of NO_2^-/sulphanilamide/H^+ (red spectrum, Fig. 2E) displayed a new characteristic IR peak at 1550 cm^{-1} corresponding to N=N stretching,[92] which unambiguously revealed the formation of the diazo compound in the synthesized gel network. Furthermore, the appearance of additional IR peaks at 1380 cm^{-1} and 1170 cm^{-1} corresponding to S=O (asymmetric and symmetric) stretching modes[93] supported the successful coupling of the sulphanilamide-derived diazonium ion with the immobilized aniline. No such IR peaks were observed for AMFG prior to the Griess reaction (blue spectrum, Fig. 2E). Furthermore, detailed absorption and fluorescence spectral analysis

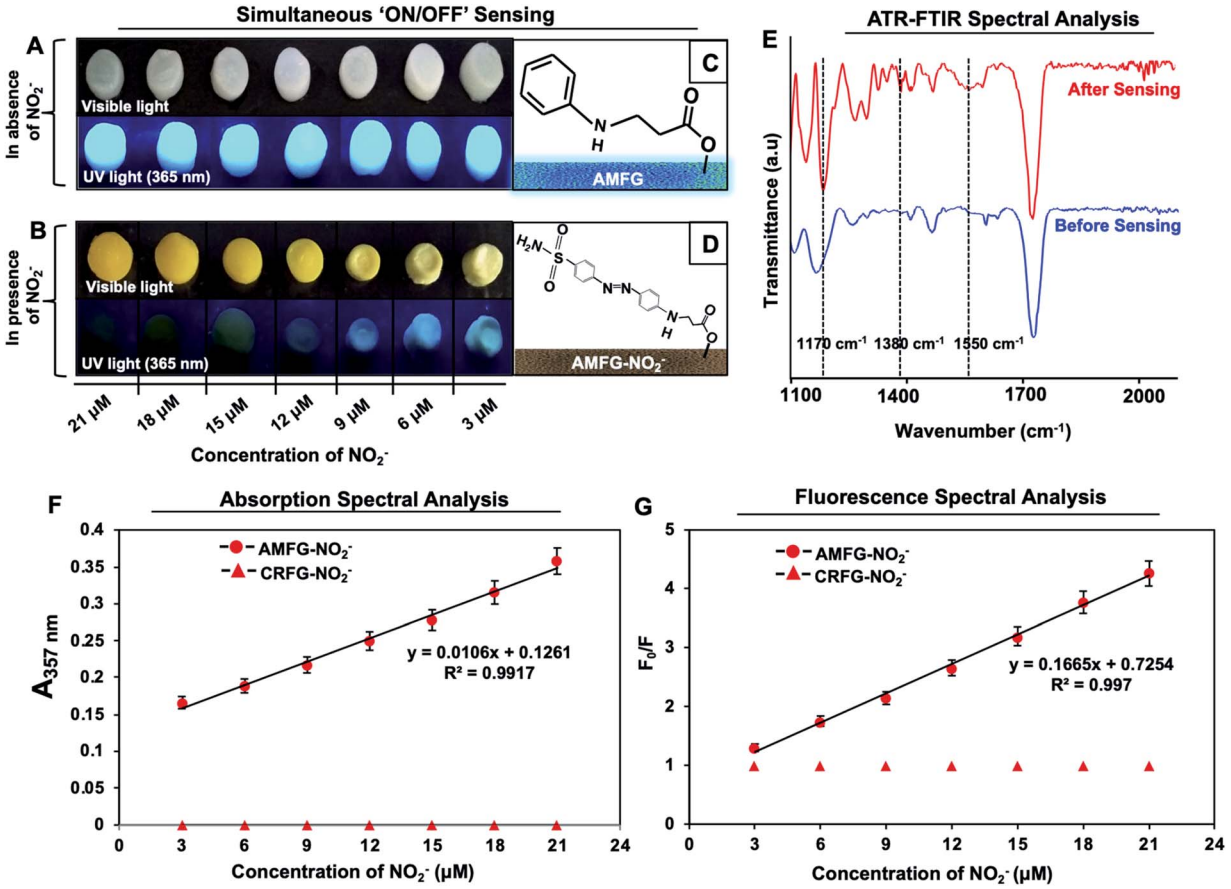

Fig. 2 Digital images of AMFG under visible and UV light (365 nm) (A) before and (B) after the parallel colorimetric and fluorimetric 'ON'/'OFF' sensing of different concentrations of NO_2^-. (C and D) Schematic diagrams depicting the changes in the chemistry of AMFG before (C) and after (D) NO_2^- sensing. (E) Comparative ATR-FTIR spectral analysis of AMFG before and after NO_2^- sensing. (F) A plot illustrating the change in the absorbance of AMFG at different concentrations of NO_2^-. (G) A Stern–Volmer plot for the quenching of the fluorescence intensity of AMFG by NO_2^-. CRFG prior to post-covalent modification with aniline was used as the blank control; this material failed to provide any optical response (UV-vis absorbance, (F) and fluorescence signal, (G) red triangles) towards NO_2^- under an experimental set-up identical to that adopted for AMFG.

allowed the amount of NO_2^- present in the samples to be quantified. For example, solid-state UV-visible absorption spectra of AMFG were recorded after performing the Griess reaction with different concentrations of NO_2^-. As expected, the UV absorbance at 357 nm gradually increased as the concentration of NO_2^- was varied from 3 μM to 21 μM, as shown in Fig. 2F. The recorded UV absorbance values followed the Beer–Lambert law and were fitted well to a straight line with a R^2 value of 0.9917, as shown in Fig. 2F. Thus, this colorimetric change allowed the quantification of unknown concentrations of nitrite using AMFG. Simultaneously, the solid-state fluorescence signal of AMFG was gradually quenched in the presence of different concentrations of NO_2^- (3–21 μM) during the Griess reaction (Scheme 2). The quenching of the fluorescence signal of AMFG before and after the Griess reaction with increasing concentration of NO_2^- followed the standard Stern–Volmer equation (eqn (1)).

$$F_0/F = 1 + K_{SV}[Q] \quad (1)$$

where F_0 and F are the fluorescence signals of AMFG before and after the Griess reaction (Scheme 2), K_{SV} is the quenching constant and [Q] is the concentration of the quencher, in this case, nitrite. The widely accepted Stern–Volmer plot of the change in the fluorescence signal (F_0/F) *versus* the concentration of NO_2^- is presented in Fig. 2G. The change in the fluorescence signal ratio before and after the Griess reaction exhibited a linear relationship with the variation in the concentration of nitrite ions ($R^2 = 0.997$). This fluorimetric calibration process also provided a parallel and distinct basis for the quantitative estimation of nitrite. In the presence of nitrite ions (15 μM), the fluorescence signal of the gel under UV light gradually decreased with time. In this study, CRFG, which lacks aniline modification, was used as the blank control; this material failed to provide any optical response towards NO_2^- under an identical experimental set-up, as is evident from Fig. 2F and G (red triangles). Further, the software ImageJ was used to monitor the decrease in the fluorescence signal from AMFG with time (Fig. S5‡). The time-lapse analysis validates the rapid, unambiguous and solid-state sensing of nitrite ions. Further, the

software ImageJ was used to estimate the corrected total fluorescence intensities directly from the photographs of AMFG under UV light before and after performing the Griess reaction. The percentage decreases in the fluorescence signal in the AMFG images (under UV light) as a function of different concentrations of NO_2^- are presented in Fig. S6.‡ The changes in the fluorescence signal of AMFG in the presence of different concentrations of NO_2^- were investigated using two distinct methods: (1) fluorescence spectroscopy and (2) analysis of digital photographs using the software ImageJ, as shown in Fig. S6B.‡ The fluorescence spectra in Fig. S6A‡ demonstrates the gradual decrease in the fluorescence signal of AMFG with increasing concentration of NO_2^- in the 3–21 μM range. The decrease in the fluorescence signal was expressed as the percentage change in the fluorescence (blue bars in Fig. S6B‡). Furthermore, a very similar change in the fluorescence signal was obtained from the ImageJ software analysis of the digital photographs of the gel under UV light as the concentration of NO_2^- was increased from 3 μM to 21 μM, as shown in Fig. S6B‡ (red bars). Thus, this simple digital photograph analysis process allows the detection of nitrite far below the permitted level without the use of sophisticated instrumentation. Additionally, a control experiment was designed to examine the importance of the aniline modification of CRFG in the current design of a simultaneous 'ON'/'OFF' sensing system in the solid-state. Without the post-covalent modification with aniline, CRFG remained completely unsuitable for the simultaneous 'ON'/'OFF' sensing of NO_2^-, as shown in Fig. S7A–D.‡ No obvious colorimetric (under visible light) or fluorometric (under UV light) change was noted for CRFG, as shown in Fig. S7.‡

Selectivity of simultaneous 'ON'/'OFF' sensing

High selectivity is an important and highly desirable feature for the prospective application of any sensor in practically relevant settings. In the current study, the simultaneous fluorimetric and colorimetric sensing of nitrite by AMFG was investigated in the presence of a series of interfering ions that often coexist with NO_2^- in all of its possible sources. No colorimetric or fluorometric changes in AMFG were observed after its individual exposure to various interfering ions, including Cl^-, Br^-, NO_3^-, CO_3^{2-}, SO_4^{2-} and PO_4^{3-}, in the presence of sulfanilamide in acidic media, as shown in Fig. 3B; the concentration of each interfering ion was set to be significantly high (1 mM). The AMFG remained white under visible light and its fluorescence signal remained unperturbed, as shown in Fig. 3B, likely due to the inability of these interfering ions to form the essential diazonium ion. However, an apparent change in the coloration of the native gel from white to intense yellow was noted under visible light upon the exposure of the AMFG to NO_2^- (9 μM) in the presence of separate mixtures of the individual interfering ions (1 mM) and sulfanilamide in acidic media as shown in Fig. 3C. As expected, significant quenching of the fluorescence intensity of AMFG was also simultaneously observed. Additionally, the colorimetric and fluorometric changes of AMFG in both the presence and absence of interfering ions were quantified by measuring its UV absorption and fluorescence in the solid state, as shown in Fig. 3D and E. This simple demonstration revealed the minimal impact of the

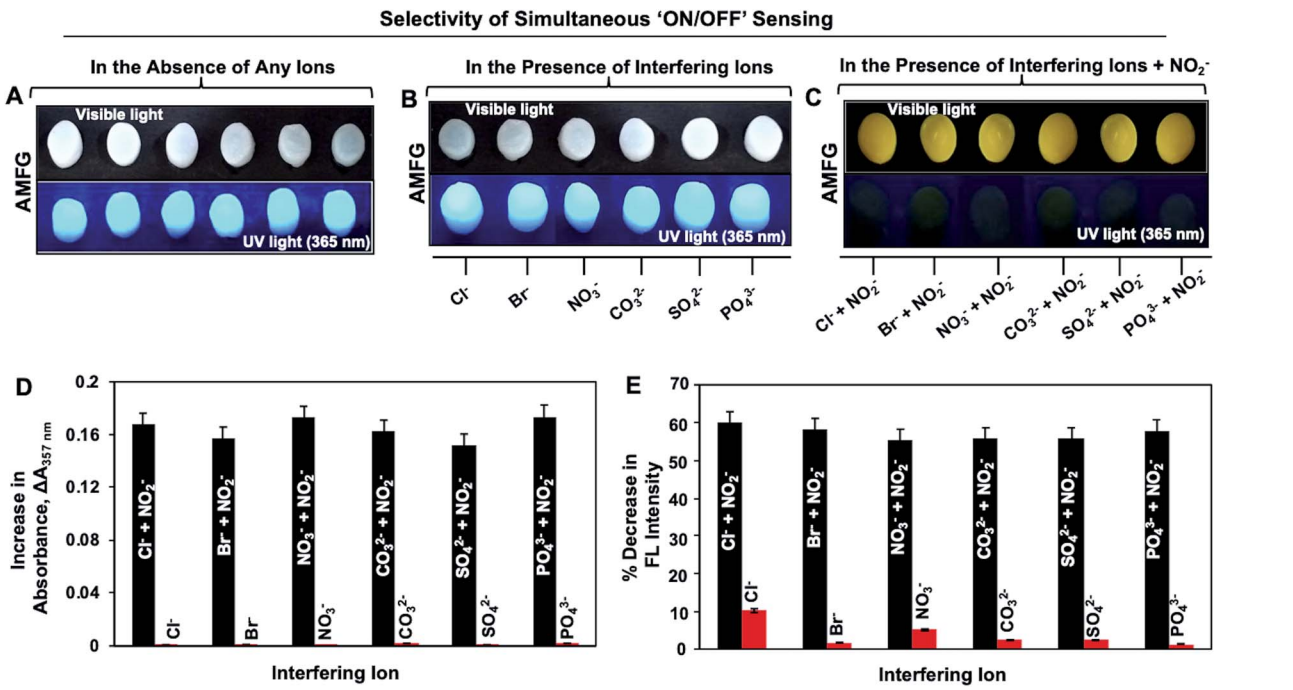

Fig. 3 Digital photographs of AMFG under visible and UV light (A) in the absence of any ions, (B) in the presence of individual interfering ions, and (C) in the presence of individual interfering ions with NO_2^-. Histogram plots demonstrating the (D) comparative increase in the absorbance of AMFG at 357 nm and (E) the comparative decrease (in %) in the fluorescence intensity of AMFG in the presence of individual interfering ions and mixtures of individual interfering ions and NO_2^-.

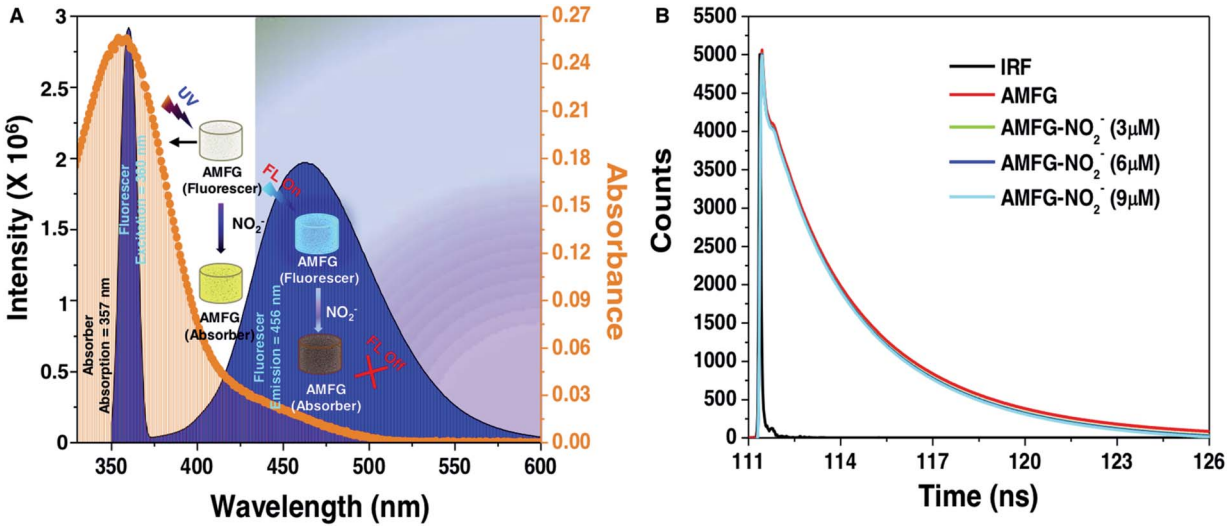

Fig. 4 (A) Absorbance and emission spectra of AMFG showing significant spectral overlap. (B) Fluorescence lifetime decay curves of AMFG in the absence and presence of different concentrations of NO_2^-.

relevant interfering ions on the sensing of nitrite by AMFG. Further experiments were designed to demonstrate the feasibility of the sensor for NO_2^- sensing in practical settings. Both tap water and deionized (DI) water were separately contaminated with known concentrations of NO_2^- (denoted as sample 1, sample 2 and sample 3 in Fig. S8‡). The developed sensor was used to experimentally quantify and compare the concentrations of NO_2^- present in either the DI water or tap water, as shown in Fig. S8.‡

Plausible mechanisms for the colorimetric and fluorometric changes in the AMFG in presence of nitrite ions were then considered in detail. The formation of the diazo compound in AMFG through the coupling of the diazonium ion with the covalently immobilized aniline led to the yellow coloration of the synthesized gel. Eventually, a broad absorption over a wide wavelength range from 325 nm to 500 nm with an absorption maximum at 357 nm appeared, as shown in Fig. 4A (orange spectrum). Careful analysis of the absorption/emission spectra and measurements of fluorescence lifetime allowed a plausible mechanism for the fluorescence quenching to be developed. There are different static and dynamic processes for fluorescence quenching, including the formation of a ground-state electrostatic complex, Forster resonance energy transfer (FRET) and the inner filter effect (IFE). In order to ascertain the exact quenching mechanism, the fluorescence quenching of AMFG by NO_2^- in the presence of sulphanilamide (in acidic media) was analyzed in detail. The formation of a ground-state electrostatic complex is relatively unlikely in the current design, as the diazonium ion was covalently coupled with covalently immobilized aniline in the porous AMFG. However, the good spectral overlap between the absorption spectrum of the quencher and the corresponding absorption/emission spectrum of the fluorescer suggested that the fluorescence quenching follows either a FRET or an IFE process. Under excitation at 360 nm, AMFG exhibited a strong fluorescence emission peak at 457 nm (blue spectrum, Fig. 4A). Furthermore, the potential quenching mechanism was analyzed carefully using time-resolved fluorescence spectrometry. The fluorescence lifetime is known to change proportionally with the concentration of the quencher in dynamic quenching but remain constant in static quenching. The fluorescence lifetime of AMFG was found to be 3.425 ns in the absence of NO_2^-. In the presence of different concentrations (3 μM, 6 μM and 9 μM) of NO_2^-, the fluorescence lifetimes were estimated to be 3.397 ns, 3.372 ns and 3.367, respectively. No apparent change in the fluorescence lifetime was noted with the change in the concentration of analytes, as shown in Fig. 4B. Thus, the fluorescence lifetime measurements ruled out the possibility of fluorescence quenching through FRET in AMFG. Subsequently, the Stern–Volmer equation (eqn (1)) was used to explain the fluorescence quenching pathways. The approximate value of quenching constant, K_{SV}, calculated from the slope of the regression line of the Stern–Volmer plot (Fig. 2G) was $1.665 \times 10^5\ M^{-1}$, and the corresponding value of k_q was calculated to be $4.857 \times 10^{13}\ M^{-1}\ s^{-1}$ from the fluorescence lifetime of AMFG (3.425 ns) and K_{SV} using eqn (1). It should be noted that the k_q value obtained is much higher than the possible value for a dynamic quenching effect ($1.0 \times 10^{10}\ M^{-1}\ s^{-1}$)[94] Thus, taken together, the fluorescence lifetime data, high quenching rate constant, and absorption/emission spectral overlap of the absorber and fluorescer indicate IFE as the probable pathway for the quenching of the fluorescence in AMFG. Thus, this report provides a fundamentally different and simple approach to integrate both chemical reactivity and luminescence. This approach has the potential to provide various functional materials through the strategic and appropriate modulation of the chemistry of the luminescent interface.

Conclusions

In conclusion, a chemically reactive, highly fluorescent gel was synthesized *via* the strategic and covalent integration of BPEI-

derived carbon dots through a 1,4-conjugate addition reaction between amine and acrylate functional groups under ambient conditions. This simple chemical approach prevented the unwanted aggregation-induced quenching of fluorescence that is generally observed in the solution phase. Furthermore, the resulting chemically reactive and fluorescent gel (CRFG) was employed to develop a portable and parallel 'ON'/'OFF' sensor for a relevant toxic chemical that does not require a sophisticated instrumental set-up. The post-covalent modification of CRFG with aniline allowed for the selective synthesis of a diazo compound in the porous gel network *via* a modified Griess reaction. This aniline-modified gel remained highly fluorescent and provided a facile basis for the unambiguous and simultaneous 'ON'/'OFF' detection of nitrite with high selectivity and sensitivity (below 10 μM; far below the permissible level (65 μM) set by the WHO). This chemical sensing remained unaffected, even in the presence of various relevant interfering agents. This chemically reactive fluorescent interface would be useful for incorporating various desired chemistries, and the strategic chemical modification of the fluorescent gel would enable the development of various functional and smart interfaces.

Conflicts of interest

There are no conflicts to declare.

Acknowledgements

Financial support from the Department of Biotechnology (BT/PR21251/NNT/28/1067/2016) is acknowledged. We acknowledge support from the Ministry of Electronics and Information Technology (grant no. 5(9)/2012-NANO). We thank CIF and the Department of Chemistry, Indian Institute of Technology-Guwahati, for their generous help. Upama Baruah is thankful to IIT G for her postdoctoral fellowship.

References

1 M. E. Buck, J. Zhang and D. M. Lynn, *Adv. Mater.*, 2007, **19**, 3951.
2 M. E. Buck, A. S. Breitbach, S. K. Belgrade, H. E. Blackwell and D. M. Lynn, *Biomacromolecules*, 2009, **10**, 1564.
3 H. Chen and J. Lahann, *Langmuir*, 2011, **27**, 34.
4 F. Bally, K. Cheng, H. Nandivada, X. Deng, A. M. Ross, A. Panades and J. Lahann, *ACS Appl. Mater. Interfaces*, 2013, **5**, 9262.
5 A.-L. Winkler, M. Koenig, A. Welle, V. Trouillet, D. Kratzer, C. Hussal, J. Lahann and C. Lee-Thedieck, *Biomacromolecules*, 2017, **18**, 3089.
6 J. M. Spruell, M. Wolffs, F. A. Leibfarth, B. C. Stahl, J. Heo, L. A. Connal, J. Hu and C. J. Hawker, *J. Am. Chem. Soc.*, 2011, **133**, 16698.
7 R. Manova, T. A. Van-Beek and H. Zuilhof, *Angew. Chem., Int. Ed.*, 2011, **50**, 5428.
8 A. H. Broderick, M. R. Lockett, M. E. Buck, Y. Yuan, L. M. Smith and D. M. Lynn, *Chem. Mater.*, 2012, **24**, 938.
9 S. L. Bechler and D. M. Lynn, *Biomacromolecules*, 2012, **13**, 1523.
10 U. Manna, A. H. Broderick and D. M. Lynn, *Adv. Mater.*, 2012, **24**, 4291.
11 J. Li, L. Li, X. Du, W. Feng, A. Welle, O. Trapp, M. Grunze, M. Hirtz and P. A. Levkin, *Nano Lett.*, 2015, **15**, 675.
12 U. Manna and D. M. Lynn, *Adv. Funct. Mater.*, 2015, **25**, 1672.
13 M. C. D. Carter and D. M. Lynn, *Chem. Mater.*, 2016, **28**, 5063.
14 A. M. Rather and U. Manna, *Chem. Mater.*, 2016, **28**, 8689.
15 M. C. D. Carter, J. Jennings, F. W. Speetjens, D. M. Lynn and M. K. A. Mahanthappa, *Macromolecules*, 2016, **49**, 6268.
16 A. M. Rather, S. Mahato, K. Maji, N. Gogoi and U. Manna, *Nanoscale*, 2017, **9**, 16154.
17 S. M. M. Dadfar, S. Sekula-Neuner, U. Bog, V. Trouillet and M. Hirtz, *Small*, 2018, **14**, 1800131.
18 J. Atwater, D. S. Mattes, B. Streit, C. von Bojničić-Kninski, F. F. Loeffler, F. Breitling, H. Fuchs and M. Hirtz, *Adv. Mater.*, 2018, **30**, 1801632.
19 N. Jana, D. Parbat, B. Mondal, S. Das and U. Manna, *J. Mater. Chem. A*, 2019, **7**, 9120.
20 H. Li, R. Liu, S. Lian, Y. Liu, H. Huang and Z. Kang, *Nanoscale*, 2013, **5**, 3289.
21 D.-W. Zhang, N. Papaioannou, N. M. David, H. Luo, H. Gao, L. C. Tanase, T. Degousée, P. Samorì, A. Sapelkin, O. Fenwick, M.-M. Titirici and S. Krause, *Mater. Horiz.*, 2018, **5**, 423.
22 W. Kwon, S. Do, J. Lee, S. Hwang, J. K. Kim and S.-W. Rhee, *Chem. Mater.*, 2013, **25**, 1893.
23 S. M. Ardekani, A. Dehghani, P. Ye, K.-A. Nguyen and V. G. Gomes, *J. Colloid Interface Sci.*, 2019, **552**, 378.
24 L. Zhou, Z. Li, Z. Liu, J. Ren and X. Qu, *Langmuir*, 2013, **29**, 6396.
25 Q. Zeng, D. Shao, X. He, Z. Ren, W. Ji, C. Shan, S. Qu, J. Li, L. Chen and Q. Li, *J. Mater. Chem. B*, 2016, **4**, 5119.
26 P. Mirtchev, E. J. Henderson, N. Soheilnia, C. M. Yipc and G. A. Ozin, *J. Mater. Chem.*, 2012, **22**, 1265.
27 Y. Zhu, X. Ji, C. Pan, Q. Sun, W. Song, L. Fang, Q. Chen and C. E. Banks, *Energy Environ. Sci.*, 2013, **6**, 3665.
28 H. Nie, M. Li, Q. Li, S. Liang, Y. Tan, L. Sheng, W. Shi and S. X.-A. Zhang, *Chem. Mater.*, 2014, **26**, 3104.
29 J. Zhao, M. Huang, L. Zhang, M. Zou, D. Chen, Y. Huang and S. Zhao, *Anal. Chem.*, 2017, **89**, 8044.
30 M. Lan, Y. Di, X. Zhu, T.-W. Ng, J. Xia, W. Liu, X. Meng, P. Wang, C.-S. Lee and W. Zhang, *Chem. Commun.*, 2015, **51**, 15574.
31 T. T. Bui and S.-Y. Park, *Green Chem.*, 2016, **18**, 4245.
32 S. Mandani, B. Sharma, D. Dey and T. K. Sarma, *Nanoscale*, 2015, **7**, 1802.
33 V. A. Ansi and N. K. Renuka, *Sens. Actuators, B*, 2018, **264**, 67.
34 C.-L. Shen, J.-H. Zang, Q. Lou, L.-X. Su, Z. Li, Z.-Y. Liu, L. Dong and C.-X. Shan, *Carbon*, 2018, **136**, 359.
35 S. Qu, X. Wang, Q. Lu, X. Liu and L. Wang, *Angew. Chem., Int. Ed.*, 2012, **51**, 12215.
36 H. Wang, J. Di, Y. Sun, J. Fu, Z. Wei, H. Matsui, A. C. Alonso and S. Zhou, *Adv. Funct. Mater.*, 2015, **25**, 5537.

37 Z. Tian, X. Zhang, D. Li, D. Zhou, P. Jing, D. Shen, S. Qu, R. Zboril and A. L. Rogach, *Adv. Opt. Mater.*, 2017, **5**, 1700416.

38 A. Cayuela, S. R. Kennedy, M. L. Soriano, C. D. Jones, M. Valcárcel and J. W. Steed, *Chem. Sci.*, 2015, **6**, 6139.

39 K. Jiang, L. Zhang, J. Lu, C. Xu, C. Cai and H. Lin, *Angew. Chem., Int. Ed.*, 2016, **55**, 7231.

40 S. Bhattacharya, R. S. Phatake, S. N. Barnea, N. Zerby, J.-J. Zhu, R. Shikler, N. G. Lemcoff and R. Jelinek, *ACS Nano*, 2019, **13**, 1433.

41 Y. Zhao, X. Zhao, B. Tang, W. Xu, J. Li, J. Hu and Z. Gu, *Adv. Funct. Mater.*, 2010, **20**, 976.

42 O. Kotova, R. Daly, C. M. G. Dos Santos, M. Boese, P. E. Kruger, J. J. Boland and T. Gunnlaugsson, *Angew. Chem., Int. Ed.*, 2012, **51**, 7208.

43 P. Chen, Q. Li, S. Grindy and N. Holten-Andersen, *J. Am. Chem. Soc.*, 2015, **137**, 11590.

44 A. Cayuela, S. R. Kennedy, M. L. Sorianoa, M. Valcárcel and J. W. Steed, *Chem. Sci.*, 2015, **6**, 6139.

45 A. Beneduci, S. Cospito, M. L. Deda and G. Chidichimo, *Adv. Funct. Mater.*, 2015, **25**, 1240.

46 C. Lu, M. Zhang, D. Tang, X. Yan, Z. Zhang, Z. Zhou, B. Song, H. Wang, X. Li, S. Yin, H. Sepehrpour and P. J. Stang, *J. Am. Chem. Soc.*, 2018, **140**, 7674.

47 Q. Zhu, L. Zhang, K. Van Vliet, A. Miserez and N. Holten-Andersen, *ACS Appl. Mater. Interfaces*, 2018, **10**, 10409.

48 D. M. Lynn and R. Langer, *J. Am. Chem. Soc.*, 2000, **122**, 10761.

49 S. R. Little, D. M. Lynn, Q. Ge, D. G. Anderson, S. V. Puram, J. Z. Chen, H. N. Eisen and R. Langer, *Proc. Natl. Acad. Sci. U. S. A.*, 2004, **101**, 9534.

50 G. Wang, Y. Fang, P. Kim, A. Hayek, M. R. Weatherspoon, J. W. Perry, K. H. Sandhage, S. R. Marder and S. C. Jones, *Adv. Funct. Mater.*, 2009, **19**, 2768.

51 J. Ford, S. R. Marder and S. Yang, *Chem. Mater.*, 2009, **21**, 476.

52 A. Y. Arasi, J. J. L. Jeyakumari, B. Sundaresan, V. Dhanalakshmi and R. Anbarasand, *Spectrochim. Acta, Part A*, 2009, **74**, 1229.

53 H.-H. Ren, Y. Fan, B. Wang and L.-P. Yu, *J. Agric. Food Chem.*, 2018, **66**, 8851.

54 F. Manea, A. Remes, C. Radovan, R. Podea, S. Picken and J. Schoonman, *Talanta*, 2010, **83**, 66.

55 S. S. Mirvish, *Cancer Lett.*, 1995, **93**, 17.

56 K. Nakamura, Y. Yoshida, I. Mikami and T. Okuhara, *Appl. Catal.*, 2006, **65**, 31.

57 J. D. Brender, J. M. Olive, M. Felkner, L. Suarez, W. Marckwardt and K. A. Hendricks, *Epidemiology*, 2004, **15**, 330.

58 L. Guadagnini and D. Tonelli, *Sens. Actuators, B*, 2013, **188**, 806.

59 WHO (World Health Organization), *Guidelines for Drinking-water Quality*, WHO, Geneva, 3rd edn, 2004.

60 G. Xiang, Y. Wang, H. Zhang, H. Fan, L. Fan, L. He, X. Jiang and W. Zhao, *Food Chem.*, 2018, **260**, 13.

61 W. Ning, C. Xia, C. Xiaolan, X. Yanjun and G. Lin, *Analyst*, 2010, **135**, 2106.

62 K.-P. Lee, A. I. Gopalan and S. Komathi, *Sens. Actuators, B*, 2009, **141**, 518.

63 Y. Haldorai, J. Y. Kim, A. T. E. Vilian, N. S. Heo, Y. S. Huh and Y.-K. Han, *Sens. Actuators, B*, 2016, **227**, 92.

64 W. L. Daniel, M. S. Han, J.-S. Lee and C. A. Mirkin, *J. Am. Chem. Soc.*, 2009, **131**, 6362.

65 Z. Lin, W. Xue, H. Chen and J.-M. Lin, *Anal. Chem.*, 2011, **83**, 8245.

66 X. Yin, Q. Chen, H. Song, M. Yang and H. Wang, *Electrochem. Commun.*, 2013, **34**, 81.

67 A. Buldt and U. Karst, *Anal. Chem.*, 1999, **71**, 3003.

68 J. Zhang, C. Chen, X. Xu, X. Wang and X. Yang, *Chem. Commun.*, 2013, **49**, 2691.

69 R. Gao, F. Wang, Y. Zhu and G. Li, *Supramol. Chem.*, 2016, **28**, 204.

70 H. Zhang, S. Kang, G. Wang, Y. Zhang and H. Zhao, *ACS Sens.*, 2016, **1**, 875.

71 J. Jia, W. Lu, L. Li, Y. Gao, Y. Jiao, H. Han, C. Dong and S. Shuang, *J. Mater. Chem. B*, 2020, **8**, 2123.

72 B.-L. Li, Y.-S. Lia and X.-F. Gao, *Food Chem.*, 2019, **274**, 162.

73 X. Wang, E. Adams and A. V. Schepdael, *Talanta*, 2012, **97**, 142.

74 Y. Luo, G. Wen, J. Dong, Q. Liu, A. Liang and Z. Jiang, *Sens. Actuators, B*, 2014, **201**, 336.

75 N. Xiao and C. Yu, *Anal. Chem.*, 2010, **82**, 3659.

76 Y. J. Jiang, M. Lin, T. Yang, R. S. Li, C. Z. Huang, J. Wang and Y. F. Lin, *J. Mater. Chem. B*, 2019, **7**, 2074.

77 X. Hua, J. Shia, Y. Shia, X. Zoua, H. E. Tahira, M. Holmes, W. Zhang, X. Huang, Z. Lia and Y. Xua, *Meat Sci.*, 2019, **147**, 127.

78 M. Zan, L. Rao, H. Huang, W. Xie, D. Zhu, L. Lia, X. Qie, S.-S. Guo, X.-Z. Zhao, W. Liu and W.-F. Dong, *Sens. Actuators, B*, 2018, **262**, 555.

79 L. Wang, B. Li, L. Zhang, L. Zhang and H. Zhao, *Sens. Actuators, B*, 2012, **172**, 946.

80 H. Wang, N. Wan, L. Ma, Z. Wang, B. Cui, W. Han and Y. Chen, *Analyst*, 2018, **143**, 4555.

81 J. Zhang, F. Pan, Y. Jina, N. Wang, J. He, W. Zhang and W. Zhao, *Dyes Pigm.*, 2018, **155**, 276.

82 Y.-C. Wang, Y.-C. Chen, W.-S. Chuang, J.-H. Li, Y.-S. Wang, C.-H. Chuang, C.-Y. Chen and C.-W. Kung, *ACS Appl. Nano Mater.*, 2020, **3**, 9440.

83 W. L. Daniel, M. S. Han, J.-S. Lee and C. A. Mirkin, *J. Am. Chem. Soc.*, 2009, **131**, 6362.

84 N. S. M. Noor, L. L. Tan, L. Y. Heng, K. F. Chong and S. N. Tajuddin, *Food Chem.*, 2016, **207**, 132.

85 M. Bru, M. I. Burguete, F. Galindo, S. V. Luis, M. J. Marin and L. Vigara, *Tetrahedron Lett.*, 2006, **47**, 1787.

86 P. Tapangpan, K. Panyarat, C. Chankaew, K. Grudpan and A. Rujiwatra, *Inorg. Chem. Commun.*, 2020, **111**, 1076272.

87 D. Li, Y. Ma, H. Duan, W. Deng and D. Li, *Biosens. Bioelectron.*, 2018, **99**, 389.

88 Y. Xiong, M. Li, H. Liu, Z. Xuan, J. Yang and D. Liu, *Nanoscale*, 2017, **9**, 1811.

89 C. Chen, Z. Yuan, H.-T. Chang, F. Lu, Z. Li and C. Lu, *Anal. Methods*, 2016, **8**, 2628.

90 M. H. Ibrahim, Z. Xue, H. I. Abdu, M. I. Shinger, A. M. Idris, M. M. Edris, D. Shan and X. Lu, *Nanoscale Adv.*, 2019, **1**, 1207.
91 Y. Zhang, Z. Su, B. Li, L. Zhang, D. Fan and H. Ma, *ACS Appl. Mater. Interfaces*, 2016, **8**, 12344.
92 P. J. Larkin, General Outline for IR and Raman Spectral Interpretation, *Infrared and Raman Spectroscopy: Principles and Spectral Interpretation*, 2nd edn, 2018, p. 135.
93 A. Borba, A. Gómez-Zavaglia and R. Fausto, *J. Phys. Chem. A*, 2013, **117**, 704.
94 J. R. Lakowicz, Principles of Fluorescence Spectroscopy, *Springer*, 3rd edn, 1999.